Nano Res (2009) 2: 975–983
DOI 10.1007/s12274-009-9102-z
Research Article

Interfacial Activation of Catalytically Inert Au (6.7 nm)–Fe_3O_4 Dumbbell Nanoparticles for CO Oxidation

Binghui Wu[§], Hai Zhang[§], Cheng Chen, Shuichao Lin, and Nanfeng Zheng (✉)

State Key Laboratory for Physical Chemistry of Solid Surfaces and Department of Chemistry, College of Chemistry and Chemical Engineering, Xiamen University, Xiamen 361005, China

Received: 19 September 2009 / Revised: 1 November 2009 / Accepted: 15 November 2009

ABSTRACT

Au nanoparticles epitaxially grown on Fe_3O_4 in Au (6.7 nm)–Fe_3O_4 dumbbell nanoparticles exhibit excellent stability against sintering, but display negligible catalytic activity in CO oxidation. Starting from various supported Au (6.7 nm)–Fe_3O_4 catalysts prepared by the colloidal deposition method, we have unambiguously identified the significance of the Au–TiO_2 interface in CO oxidation, without any possible size effect of Au. *In situ* thermal decomposition of TiO_2 precursors on Au–Fe_3O_4 was found to be an effective way to increase the Au–TiO_2 interface and thereby optimize the catalytic performance of TiO_2-supported Au–Fe_3O_4 dumbbell nanoparticles. By reducing the size of Fe_3O_4 from 15.2 to 4.9 nm, the Au–TiO_2 contact was further increased so that the resulting TiO_2-supported Au (6.7 nm)–Fe_3O_4 (4.9 nm) dumbbell particles become highly efficient catalysts for CO oxidation at room temperature.

KEYWORDS

Gold nanocatalysts, support effect, CO oxidation, Au–Fe_3O_4, dumbbell nanoparticles

Introduction

Gold nanoparticle-based catalysts, particularly with the particle size of gold less than 10 nm [1–11], have attracted increasing research attention since Haruta discovered the remarkable activity of supported gold nanoparticles in CO oxidation at low temperature [12, 13]. To achieve good catalytic activity and stability, gold nanoparticles are generally loaded on high-surface-area supports [1, 3, 14]. While the particle size of gold nanoparticles is important in optimizing the catalytic activity, the selection of appropriate supports has also been found critical to achieving high catalytic performance and stability of supported gold nanoparticles. In most cases, the size and support effects are likely to operate simultaneously [14], due to the lack of highly reproducible techniques for the controlled preparation of well-defined gold-nanoparticle catalysts, separation of size and support effects therefore remains a challenge [15, 16]. For example, the importance of the Au–TiO_2 interface in CO oxidation over real catalysts has been widely proposed and investigated by comparison of various supported gold nanoparticles or between supported TiO_2–supported Au nanoparticles and unsupported gold powder [17–20]. The catalysts which were

Address correspondence to nfzheng@xmu.edu.cn
[§] These authors contributed equally to this work.

compared typically had different-sized gold particles. however, such studies do not allow a distinction to be made between the Au–TiO_2 support effect and the size effect. There therefore appears to be a lack of consistency in the literature regarding the size and support effects for gold nanocatalysts [16].

Fortunately, the recently developed colloidal deposition method allows the preparation of supported gold nanoparticles with more controllable structural parameters [16, 21–24]. A significant improvement of the colloidal deposition method over previous methods is that pre-made gold nanoparticles are used as the precursors. As a result, the preparation of supported gold nanoparticles with narrow particle size distribution is possible, regardless of the size of the gold nanoparticles and the nature of the support. Using the colloidal deposition method, both pre-made Au and Au–Fe_3O_4 nanoparticles have been used as the precursors to prepare supported gold nanocatalysts in order to study the support effect in CO oxidation. In these studies, the particle size of the gold nanoparticles employed was mainly $\leqslant$ 6 nm. Within this size region, however, facile sintering of the Au nanoparticles frequently occurs [16]. These nanoparticles themselves can possess good catalytic activity for CO oxidation even if deposited on inert supports. For example, carbon-supported 6 nm Au nanoparticles have been found to be highly active for CO oxidation [25]. After simple calcination, Au (3 nm)–Fe_3O_4 dumbbell particles also displayed excellent activity for CO oxidation, however [24]. Such situations make it extremely difficult to unambiguously identify any support effects responsible for significantly promoting catalysis over supported Au nanoparticles.

The main aim of this work is to identify how the Au–TiO_2 interface influences the catalytic activity of TiO_2-supported Au nanocatalysts in CO oxidation. To distinguish the support effect from the size effect, Au nanoparticles having the size of ~6.7 nm were selected. When 6.7 nm Au nanoparticles are epitaxially grown on 15.2 nm Fe_3O_4 nanoparticles to form dumbbell nanoparticles they, if not appropriately supported, exhibit negligible catalytic activity in CO oxidation. Importantly, epitaxial growth on Fe_3O_4 endows the Au nanoparticles with significant anti-sintering properties during calcination. Therefore, Au (6.7 nm)–Fe_3O_4 (15.2 nm) dumbbell nanoparticles serve as an excellent system for us to identify any support effect in catalysis by Au nanoparticles. To first evaluate the importance of the Au–TiO_2 interface in the catalysis of CO oxidation, comparison studies were performed on Au (6.7 nm)–Fe_3O_4 (15.2 nm) particles deposited on various supports. After demonstrating the importance of the Au–TiO_2 interface, thermal decomposition of TiO_2 precursors was then employed to deposit fine TiO_2 nanoparticles on Au–Fe_3O_4, which helped to increase the contact between Au and TiO_2 and promote the catalytic performance. By decreasing the particle size of Fe_3O_4 from 15.2 to 4.9 nm, we also demonstrate at the end of the article that it is possible to convert TiO_2-supported Au (6.7 nm)–Fe_3O_4 dumbbell particles into catalysts which are highly efficient for CO oxidation at room temperature.

1. Experimental

1.1 Materials

All syntheses were carried out using commercially available reagents. $HAuCl_4 \cdot 4H_2O$ was purchased from Sinopharm Chemical Reagent Co. Ltd. *Tert*-butylamine:borane complex (TBAB, 95%), $Fe(acac)_3$, oleylamine (OAm, C_{18} content: 80%–90%), and titanium(Ⅳ) isopropoxide (TIPO, 98+%) were purchased from Acros Organics. Oleic acid (OLA) was purchased from Guangdong Xilong Chemical Co. Ltd. CO (99.99%) and N_2 (99.999%) were purchased from Linde Gas. All chemicals were used as received without further purification.

1.2 Synthesis of 6.7 nm OAm-capped Au nanoparticles

In a typical synthesis, a precursor solution of chloroform (100 mL), OAm (20 mL), and $HAuCl_4 \cdot 4H_2O$ (1 g) was prepared and stirred for 10 min in air at 30 °C. A solution containing 0.8 g (9.2 mmol) of TBAB and OAm (1 mL) in 20 mL of chloroform was mixed by sonication and added to the $HAuCl_4$–OAm mixture. Within 10 s, the solution became deep purple. The mixture was further stirred at 30 °C for 1 h before 60 mL of ethanol were

added. The Au nanoparticles were then collected by centrifugation (8500 rpm, 8 min), washed with ethanol and redispersed in chloroform (100 mL, corresponding to ~5 mg/mL).

1.3 Synthesis of Au (6.7 nm)–Fe_3O_4 (15.2 nm) dumbbell nanoparticles by conventional heating

A solution containing $Fe(acac)_3$ (70.0 mg), OLA (2.7 mL) and OAm (4.0 mL) in a Schlenk tube was heated to 180 °C within 20 min and aged at 180 °C for 10 min under a flow of N_2. 2 mL of OAm containing 5 mg of Au were then injected into the reaction mixture, followed by the addition of 1.33 mL of OLA. The solution was kept at 180 °C for another 90 min, then heated to 300 °C within 25 min and aged for 20 min. After cooling to room temperature, the particles were separated by adding ethanol, centrifuged, and redispersed into chloroform.

1.4 Synthesis of Au (6.7 nm)–Fe_3O_4 (4.9 nm) dumbbell nanoparticles by microwave heating

6.7 nm Au (5 mg), $Fe(acac)_3$ (45 mg), 1,2-hexadecanediol (50 mg), OLA (1 mL) and OAm (1.5 mL) were mixed together in a 10-mL microwave vial, sealed and stirred in a 50 °C water bath for at least 2 h before microwave irradiation. The microwave reactions were carried out in a focused single-mode microwave synthesis system (Discover, CEM, USA). The mixture was heated to 130 °C by 100 W of microwave radiation with stirring. After keeping at this temperature for 15 min, the mixture was further heated to 185 °C and aged for 30 min. After cooling to room temperature, the particles were separated by adding ethanol, centrifuged, and redispersed into chloroform.

1.5 Loading Au or Au–Fe_3O_4 nanoparticles on TiO_2, SiO_2 or activated carbon

6.7 nm Au nanoparticles were deposited on a Degussa P25 TiO_2 support to generate supported Au (2.5 wt%) catalysts through the colloidal deposition method. Typically, 1 mL of a colloidal dispersion of OAm-capped gold nanoparticles (5 Au mg/mL chloroform) was first diluted by 9 mL of chloroform to form a solution. 200 mg of TiO_2 powder were then added to the Au solution and stirred for 15 min before the solids were collected by filtration. The resulting solids were then dried at 100 °C and calcined in air at the desired temperature for 2 h to remove the organic capping agents. A similar process was used to prepare supported Au–Fe_3O_4 catalysts on fumed SiO_2 and activated carbon. In order to remove the organic surfactants, the catalysts were calcined at the desired temperature (350, 450, or 550 °C) in air for 2 h.

1.6 Thermal decomposition of TIPO on Au–Fe_3O_4 nanoparticles

As described above, the Au–Fe_3O_4 dumbbell nanoparticles in our studies were prepared by conventional or microwave heating. After the reaction mixtures were cooled to 50 °C, thermal decomposition of TIPO was performed *in situ* by directly injecting 0.6 mL of TIPO into the mixture. While the mixture obtained by conventional heating was heated to 160 °C and aged for 4 h to complete the reaction, the mixture obtained by microwave heating was heated to 185 °C and aged for 10 min. After the mixtures were cooled to room temperature, the corresponding solids were separated by adding ethanol, followed by centrifugation. The composites were then washed well with ethanol and dried at 100 °C. Before catalysis evaluation, the samples were calcined at different temperatures to remove the organic residues.

1.7 Characterization

Transmission electron microscopy (TEM), including high-resolution TEM (HRTEM) studies, were performed on a Tecnai F-30 high-resolution transmission electron microscope operating at 300 kV. X-ray diffraction (XRD) measurements were recorded on a PANalytical X'pert PRO diffractometer using Cu Kα radiation, operating at 40 kV and 30 mA. TGA traces were obtained on a Q600 SDT thermogravimetric analyzer (TA Instruments) from 30 to 700 °C with heating rate of 10 °C/min and an air flow of 100 mL/min.

1.8 Catalytic experiments

The catalytic reactions were carried out in a continuous flow fixed bed glass reactor with internal diameter of 4 mm. The reactor was heated by an electrical heater controlled by a temperature controller. 5% CO in N_2 at 10 mL/min and air at 40 mL/min

were fed to the reactor by mass-flow controllers. The composition of the reaction mixture was monitored by an online gas chromatogram equipped with an FID detector coupled with a methanizer. In each measurement, the catalyst contained the same amount (5 mg) of Au nanoparticles. For the supported catalysts prepared by the colloidal deposition method, 0.200 g of the catalysts (2.5 wt% Au) prepared by the colloidal deposition method were used in measurements. For these catalysts, the space velocity was ~15 000 $cm^3/(h{\cdot}g)$. The heights of the catalyst bed were ~5, 5, and 3 cm and the corresponding contact times were ~7.5, 7.5, and 4.5 s for TiO_2-, SiO_2-, and activated carbon- supported catalysts, respectively. For the TiO_2-supported Au–Fe_3O_4-1 or Au–Fe_3O_4-2 prepared by the thermal decomposition method, the contact time was estimated to be 0.8 s. To examine whether there is diffusion limitation in our measurements, the as-prepared catalysts were also mixed with different amounts of quartz sand for catalysis measurements. However, the reactivities of the catalysts mixed with quartz sand were identical to those of the corresponding as-prepared catalysts. We can therefore assume the absence of any diffusion limitations on the overall reactivity of the catalysts.

2. Results and discussion

Figure 1 shows two types of Au–Fe_3O_4 dumbbell nano-heterojunction particles prepared in our studies. While the gold nanoparticles in both types had the same size around 6.7 nm, the Fe_3O_4 nanoparticles intergrown with the Au nanoparticles were of different size, namely, 15.2 and 4.9 nm. The as-prepared dumbbell particles with 15.2 and 4.9 nm Fe_3O_4 nanoparticles are denoted Au–Fe_3O_4-1 and Au–Fe_3O_4-2, respectively. To prepare these Au–Fe_3O_4 particles, 6.7 nm Au nanoparticles (Fig. 1(a)) were first made in chloroform by reducing $HAuCl_4$ in the presence of OAm by *tert*-butylamine:borane complex, a reducing agent that was used recently for the preparation of monodisperse Au nanoparticles [25, 26]. These pre-made Au nanoparticles were separated and transferred into a mixed solution of OLA and OAm containing $Fe(acac)_3$. $Fe(acac)_3$ and $Fe(CO)_5$ have both previously been used as the precursors to make Au–Fe_3O_4 dumbbell nanoparticles [27, 28]. In our studies, $Fe(acac)_3$ rather than $Fe(CO)_5$ was selected as the Fe_3O_4 precursor, because $Fe(CO)_5$ is highly hazardous. The mixture containing Au nanoparticles and $Fe(acac)_3$ was then subjected to heating to allow the growth of Fe_3O_4 nanoparticles on the surface of the Au particles. Conventional heating in a Schlenk tube and microwave heating were both employed in the synthesis of Au–Fe_3O_4-1 (Fig. 1(b)) and Au–Fe_3O_4-2 (Fig. 1(c)), respectively. By using conventional heating, a high temperature (300 °C), was required to produce Au–Fe_3O_4-1 particles. It

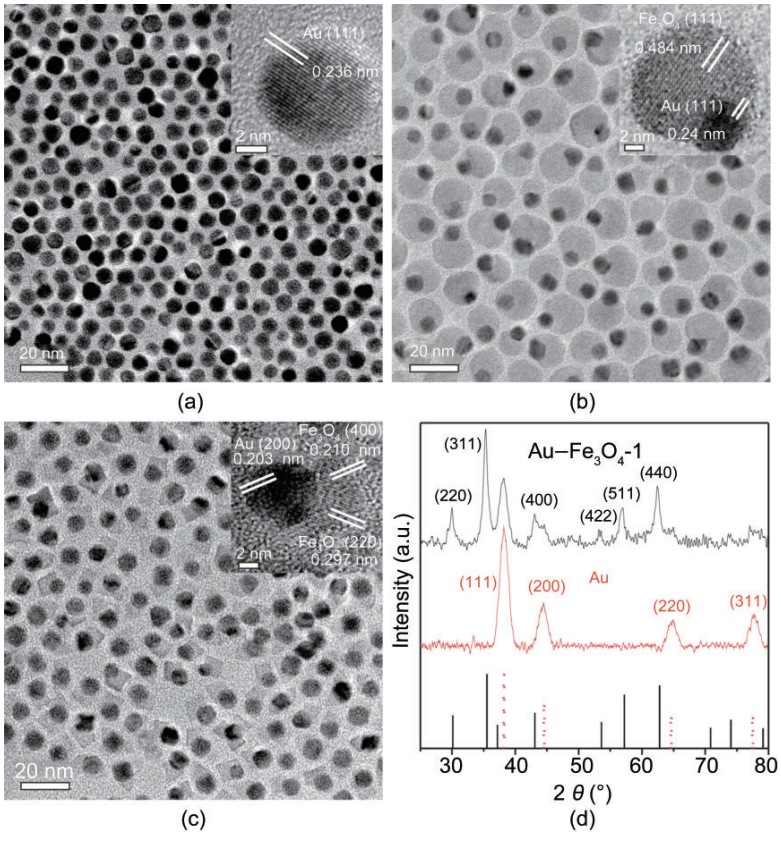

Figure 1 TEM and HRTEM images of (a) the 6.7 nm Au nanoparticles, (b) Au (6.7 nm)–Fe_3O_4 (15.2 nm) dumbbell nanoparticles prepared by conventional heating, and (c) Au (6.7 nm)–Fe_3O_4 (4.9 nm) dumbbell nanoparticles prepared by microwave heating. (d) Powder XRD patterns of as-prepared 6.7 nm Au and Au (6.7 nm)–Fe_3O_4 (15.2 nm). The standard peaks of Au and Fe_3O_4 are shown at the bottom of the figure by dotted and solid lines, respectively

should also be pointed out that in terms of ensuring that most Au particles formed hybrid particles, it was difficult to prepare Au–Fe_3O_4 dumbbell particles having smaller Fe_3O_4 particles by conventional heating. We believe that using smaller sized Fe_3O_4 particles in Au–Fe_3O_4 hybrid particles will reduce steric hindrance allowing the Au nanoparticles in dumbbell particles to make better contact with other support materials. this will be discussed later in this article. It is important to note, therefore, that by using microwave heating—a much more efficient form of heating—we have successfully synthesized Au–Fe_3O_4-2 particles having small Fe_3O_4 particles with a size of just 4.9 nm at a lower temperature (185 °C).

The inset of Fig. 1(b) shows a typical HRTEM image of an individual Au–Fe_3O_4-1 particle. Lattice fringes were clearly observed in both Au and Fe_3O_4 parts of the dumbbell particle. The distance between two adjacent planes in Fe_3O_4 was measured to be 0.484 nm, corresponding to (111) planes in the inverse spinel structured Fe_3O_4 and that in Au was 0.236 nm, resulting from the (111) planes in fcc Au. This result is consistent with the suggestion that the facile preparation of Au–Fe_3O_4 heterostructures is a result of the small lattice mismatch (~2.5%) between $2d_{111}$-(Au) and d_{111}-(Fe_3O_4) [27, 28]. The power XRD pattern (Fig. 1(d)) of the as-prepared bulk Au–Fe_3O_4-1 sample also confirmed the inverse spinel structure of Fe_3O_4 and the fcc structure of Au in the as-prepared dumbbell particles. The direct growth of the Fe_3O_4 on the Au nanoparticles is likely to reduce the mobility of Au nanoparticles and therefore prevent their facile aggregation during reactions or thermal treatments.

To support the hypothesis that the intergrowth in Au–Fe_3O_4 would help to stabilize the Au nanoparticles against aggregation, we performed comparative studies of 6.7 nm Au nanoparticles alone and Au–Fe_3O_4-1 dumbbell nanoparticles containing 6.7 nm Au nanoparticles. Both Au and Au–Fe_3O_4-1 were deposited on supports through the colloidal deposition method [23, 24]. The method allows the preparation of well-defined nanocatalysts from as-made nanoparticles, which can be hydrophobic. The deposition of organic-passivated Au and Au–Fe_3O_4-1 nanoparticles on Degussa P25 TiO_2 was carried out in chloroform. The as-deposited composites were catalytically inactive before any thermal treatment. Both Au and Au–Fe_3O_4-1 composites with TiO_2 were then calcined at 350, 450, or 550 °C to remove the organic species. As shown in Fig. 2, the sintering of Au nanoparticles in the Au/TiO_2 composite was evidenced by the formation of large Au particles

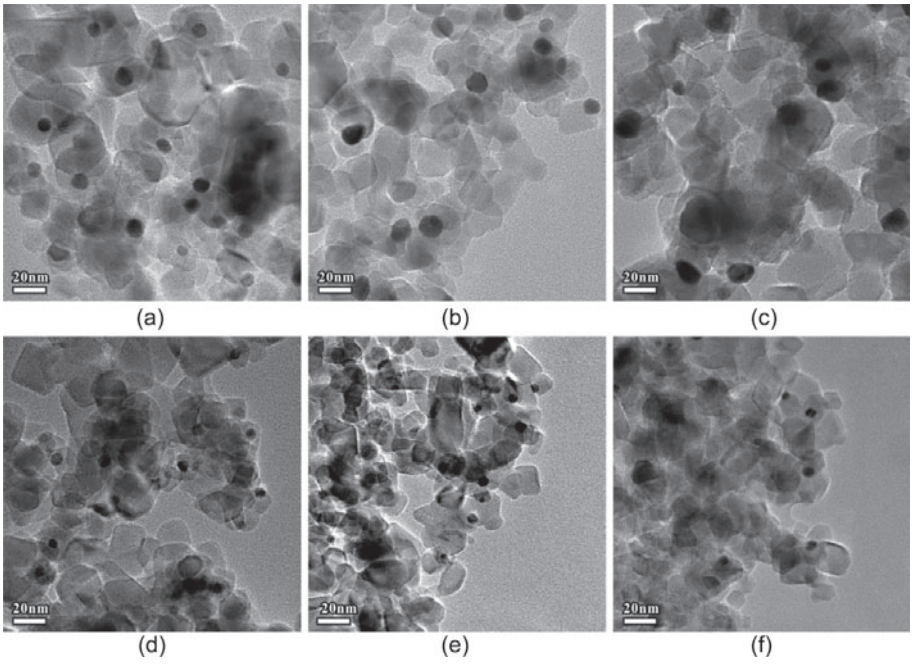

Figure 2 TEM images of Au/P25 TiO_2 calcined at (a) 350 °C, (b) 450 °C, and (c) 550 °C, and Au–Fe_3O_4-1/P25 TiO_2 calcined at (d) 350 °C, (e) 450 °C, and (f) 550 °C

(as large as 30 nm). As expected, when Au–Fe_3O_4 nanoparticles were dispersed on TiO_2, however, the Au particles retained their original size even after thermal treatment at 550 °C, suggesting that the dumbbell intergrowth structure results in a marked stabilization of the Au nanoparticles against sintering.

A similar stabilizing effect was also observed when Au–Fe_3O_4-1 particles were supported on SiO_2 or activated carbon. No sintering of the Au nanoparticles was observed, neither in SiO_2- nor in activated carbon-supported Au–Fe_3O_4-1 treated at 450 °C. Although the size of the Au nanoparticles was kept the same in all SiO_2-, TiO_2-, and C-supported Au–Fe_3O_4-1, they performed differently in the catalytic oxidation of CO as shown in their light-off curves (Fig. 3(c)). While carbon-supported Au–Fe_3O_4-1 displayed negligible activity, TiO_2-supported Au–Fe_3O_4-1 exhibited the best performance of the three supported catalysts, indicating a significant support effect on the activity of supported Au–Fe_3O_4-1. It is worth mentioning that when Au–Fe_3O_4-1 itself was calcined at 450 °C, it showed no catalytic activity for CO oxidation. These results are in remarkable contrast to what has been previously observed for the Au–Fe_3O_4 dumbbell particles having 3 nm Au nanoparticles, which easily achieved 100% CO conversion at temperatures lower than 60 °C, with or without any other support [24]. According to the size-dependent studies by Haruta and Goodman [1–3, 5, 29], the activity of supported Au nanoparticles should sharply decrease when their size is above 6 nm. Our results were reasonably consistent with such a size model.

Together with their lack of catalytic activity, the capability of stabilizing Au nanoparticles against sintering makes the dumbbell Au–Fe_3O_4 particles having 6.7 nm Au nanoparticles an excellent system to study the support effect without there being any possible influence from the size effect. Based on the above support-dependent studies, we propose that the built-in Au–TiO_2 interface is essential to activate the dumbbell Au–Fe_3O_4 particles having 6.7 nm Au nanoparticles for CO oxidation. The importance of the Au–TiO_2 interface is further supported by comparison of TiO_2-supported Au–Fe_3O_4-1 samples calcined at different temperatures (350, 450, and 550 °C). While the size of Au nanoparticles remained the same, the catalytic activity of the TiO_2-supported materials decreased with calcination temperature (Fig. 3(d)). This result can be reasonably explained by the higher degree of Au–TiO_2 interface breakage at higher calcination temperature.

Since the catalytic activity of TiO_2-supported Au–Fe_3O_4-1 was correlated with the Au–TiO_2 interface, this suggested the possibility of enhancing the catalytic performance of Au–Fe_3O_4-1 particles by enlarging the Au–TiO_2 interface. To maximize the interfacial contact between the Au nanoparticles in Au–Fe_3O_4-1 and TiO_2, we attempted to introduce TiO_2 by the *in situ* thermal decomposition of a precursor (TIPO). Following the thermal decomposition, the as-made TiO_2–Au

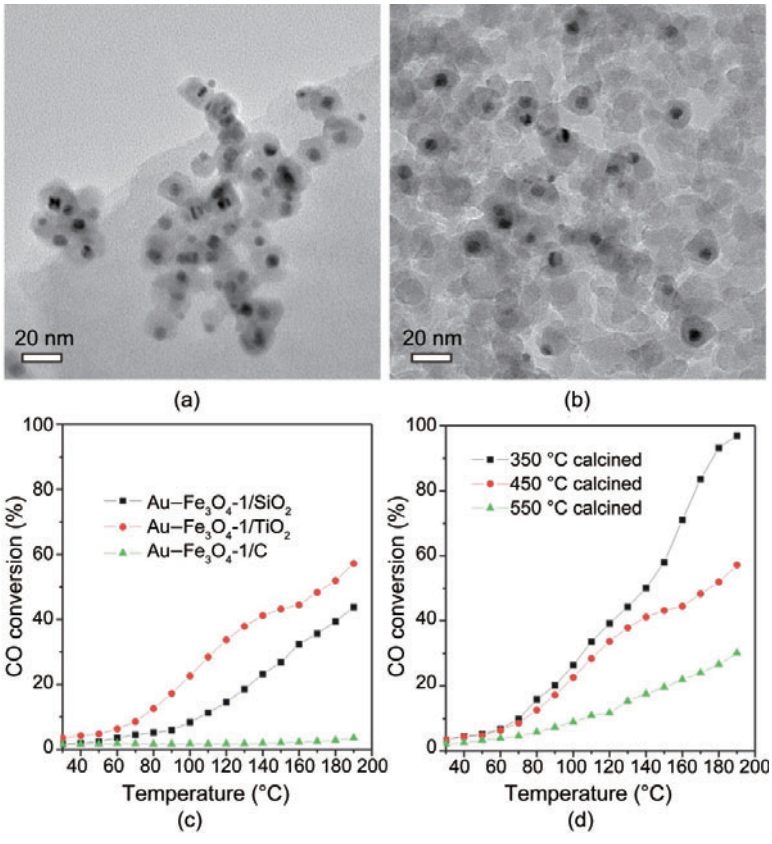

Figure 3 TEM images of (a) activated carbon- and (b) SiO_2-supported Au–Fe_3O_4-1 (calcined at 450 °C). CO oxidation conversion light-off curves of the Au nanocatalysts (c) with different supports (calcined at 450°C) and (d) supported on P25 TiO_2 with different treatment temperatures

–Fe_3O_4-1 composites were subjected to thermal treatments at 350, 450, and 550 °C. As illustrated in Figs. 4(a)–4(c), again no aggregate growth of the Au nanoparticles was observed in the all cases, confirming the stabilizing effect conferred by the intergrowth between Au and Fe_3O_4 in the dumbbell structure. The TEM images also clearly show that the particle size of TiO_2 increased with the thermal treatment temperature. Based on the TEM observations, the sample treated at 350°C should have the maximum Au –TiO_2 interfacial contact and therefore the best catalytic performance in CO oxidation. The catalytic tests, however, showed that the composites treated at 450 °C showed the best activity (Fig. 4(d)). Although our XRD studies also confirmed the increase in anatase TiO_2 crystallite size with treatment temperature (Fig. 4(e)), the TGA curve (Fig. 4(f)) for the as-prepared untreated TiO_2–Au–Fe_3O_4-1 composites revealed that a large amount of organic residue remained when the sample was treated at 350 °C. OLA present during the thermal decomposition might account for such organic residues. Undoubtedly, the presence of organic species on the TiO_2 surface was deleterious to the effective contact of the Au nanoparticles with TiO_2 and therefore to the overall catalytic performance of the composites. In contrast to thermal treatment at 350 °C, treatment at 450 °C for 2 h in air completely removed the organic residues and resulted in good Au–TiO_2 contact. When further thermally treated at 550 °C, TiO_2 grew into larger particles, leading to the loss of the Au –TiO_2 interface. Therefore, the fact that the catalytic performance of the composites treated at 450 °C was better than that of those treated at either 350 or 550° C can be nicely explained in the term of the Au–TiO_2 interfacial contact. Importantly, the thermal deposition of TiO_2 precursors was found more effective than colloidal decomposition in creating an Au–TiO_2 interface on the Au–Fe_3O_4 dumbbell particles.

While all the observations discussed above support the importance of the Au–TiO_2 interface in

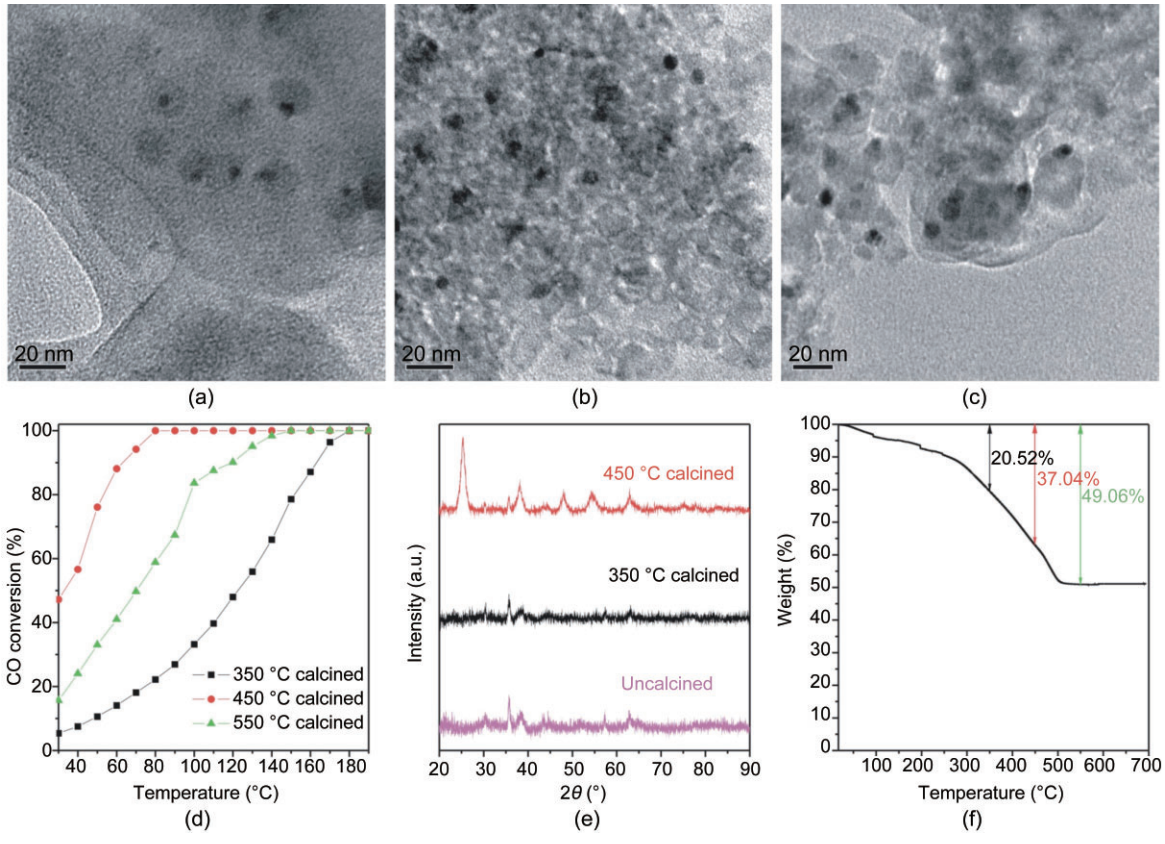

Figure 4 TEM images of Au–Fe_3O_4-1/TiO_2 prepared by *in situ* thermal decomposition of 0.6 mL TIPO and calcined at (a) 350 °C, (b) 450 °C, and (c) 550 °C. (d) CO oxidation conversion light-off curves of the Au–Fe_3O_4-1/TiO_2 nanocatalysts shown in (a)–(c). (e) XRD pattern of Au–Fe_3O_4/TiO_2 prepared by thermal decomposition and calcined at different temperatures. (f) TGA curve of Au–Fe_3O_4-1/TiO_2 catalyst prepared by thermal decomposition of 0.6 mL TIPO and dried at 100 °C

activating Au–Fe_3O_4 dumbbell particles having 6.7 nm Au nanoparticles for CO oxidation, we have found difficulty in converting Au–Fe_3O_4-1 particles into catalysts that are as efficient as supported Au nanoparticles having a smaller size. The main factor hindering us in achieving this is the large size of the Fe_3O_4 particles in Au–Fe_3O_4-1 which results in significant steric hindrance to contact between Au nanoparticles and TiO_2 in the dumbbell particles. To resolve this steric problem, it is desirable to make dumbbell particles containing smaller Fe_3O_4 nanoparticles. As discussed above, microwave heating has helped to achieve the synthesis of such dumbbell particles (Au–Fe_3O_4-2) having 4.9 nm Fe_3O_4 nanoparticles. As shown in Fig. 5(a), when Au–Fe_3O_4-2 was thermally treated with 20 μL of TIPO under microwave heating followed by calcination at 350 °C, the size of Au particles was maintained. Au–Fe_3O_4-2 was also highly dispersed on TiO_2. The as-prepared catalysts exhibited high catalytic activity of CO oxidation at 30 °C with 100% CO conversion (Fig. 5(b)). Therefore, the TiO_2-supported Au–Fe_3O_4-2 particles have both high catalytic activity and high stability. No decline in the catalytic performance of the calcined TiO_2–Au–Fe_3O_4-2 was observed up to 6 h. In comparison, the activated carbon-supported Au–Fe_3O_4-2 calcined at 350 °C exhibited much lower activity. However, compared with Au–Fe_3O_4-1, Au–Fe_3O_4-2 supported on activated carbon displayed an improved catalytic performance. Therefore, at this point, even though we can confirm the important role of the smaller size of Fe_3O_4 nanoparticles in enlarging the Au–TiO_2 contact (Fig. S-1), it is not possible to exclude a contribution from the morphology and size of the Fe_3O_4 nanoparticles to the overall catalytic performance of TiO_2–Au–Fe_3O_4-2. Further work is now in progress to elucidate the effect of the morphology and size of Fe_3O_4 in Au–Fe_3O_4 hybrid nanoparticles on their catalytic performance.

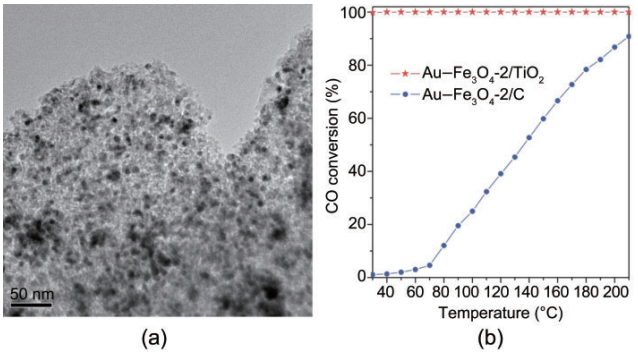

Figure 5 (a) TEM image of Au–Fe_3O_4-2/TiO_2 prepared by thermal decomposition under microwave irradiation and calcined at 350 °C. (b) CO oxidation conversion light-off curves of the Au–Fe_3O_4-2/TiO_2 nanocatalyst shown in (a) and activated carbon-supported Au–Fe_3O_4-2 calcined at 350 °C

3. Conclusions

Au (6.7 nm)–Fe_3O_4 dumbbell nanoparticles have been demonstrated to be an excellent system to study the Au metal–oxide support effect without any possible influence of the size effect of Au. Using Au (6.7 nm)–Fe_3O_4 dumbbell nanoparticles as the precursors for catalyst preparation, we have revealed the importance of the Au–TiO_2 interface in CO oxidation. The Au–TiO_2 interface was increased by depositing TiO_2 on Au–Fe_3O_4 by *in situ* thermal decomposition of TiO_2 precursors, which helped to optimize the catalytic performance by supported Au–Fe_3O_4 particles. By utilizing the Au–TiO_2 support effect, the catalytically inert Au (6.7 nm)–Fe_3O_4 dumbbell nanoparticles can be converted into catalysts which are highly efficient for CO oxidation at room temperature.

Acknowledgements

We thank the National Natural Science Foundation of China (Nos. 20871100, 20721001), and a Distinguished Young Investigator Grant (No. 20925103), Research Fund for the Doctoral Program of Higher Education of China (No. 200803841010), Natural Science Foundation of Fujian for a Distinguished Young Investigator Grant (No. 2009J06005) and the Key Scientific Project of Fujian Province (No. 2009HZ0002-1).

Electronic Supplementary Material: Supplementary material is available in the online version of this article at http://dx.doi.org/10.1007/s12274-009-9102-z and is accessible free of charge.

References

[1] Haruta, M. Catalysis of gold nanoparticles deposited on

metal oxides. *Cattech* **2002**, *6,* 102–115.

[2] Haruta, M. When gold is not noble: Catalysis by nanoparticles. *Chem. Rec.* **2003**, *3,* 75–87.

[3] Haruta, M. Gold as a novel catalyst in the 21st century: Preparation, working mechanism and applications. *Gold Bull.* **2004**, *37,* 27–36.

[4] Bond, G. C.; Thompson, D. T. Catalysis by gold. *Catal. Rev. -Sci. Eng.* **1999**, *41,* 319–388.

[5] Chen, M. S.; Goodman, D. W. The structure of catalytically active gold on titania. *Science* **2004**, *306,* 252–255.

[6] Hughes, M. D.; Xu, Y. J.; Jenkins, P.; McMorn, P.; Landon, P.; Enache, D. I.; Carley, A. F.; Attard, G. A.; Hutchings, G. J.; King, F. et al. Tunable gold catalysts for selective hydrocarbon oxidation under mild conditions. *Nature* **2005**, *437,* 1132–1135.

[7] Hashmi, A. S. K.; Hutchings, G. J. Gold catalysis. *Angew. Chem. Int. Ed.* **2006**, *45,* 7896–7936.

[8] Corma, A.; Garcia, H. Supported gold nanoparticles as catalysts for organic reactions. *Chem. Soc. Rev.* **2008**, *37*, 2096–2126.

[9] Corma, A.; Serna, P. Chemoselective hydrogenation of nitro compounds with supported gold catalysts. *Science* **2006**, *313,* 332–334.

[10] Grirrane, A.; Corma, A.; Garcia, H. Gold-catalyzed synthesis of aromatic azo compounds from anilines and nitroaromatics. *Science* **2008**, *322,* 1661–1664.

[11] Turner, M.; Golovko, V. B.; Vaughan, O. P. H.; Abdulkin, P.; Berenguer-Murcia, A.; Tikhov, M. S.; Johnson, B. F. G.; Lambert, R. M. Selective oxidation with dioxygen by gold nanoparticle catalysts derived from 55-atom clusters. *Nature* **2008**, *454,* 981–983.

[12] Haruta, M.; Kobayashi, T.; Sano, H.; Yamada, N. Novel gold catalysts for the oxidation of carbon monoxide at a temperature far below 0 °C. *Chem. Lett.* **1987**, *16,* 405–408.

[13] Haruta, M.; Yamada, N.; Kobayashi, T.; Iijima, S. Gold catalysts prepared by coprecipitation for low-temperature oxidation of hydrogen and of carbon monoxide. *J. Catal.* **1989**, *115,* 301–309.

[14] Haruta, M. Size- and support-dependency in the catalysis of gold. *Catal. Today* **1997**, *36,* 153–166.

[15] Ma, Z.; Overbury, S. H.; Dai, S. Au/M_xO_y/TiO_2 catalysts for CO oxidation: Promotional effect of main-group, transition, and rare-earth metal oxide additives. *J. Mol. Catal. A-Chem.* **2007**, *273,* 186–197.

[16] Comotti, M.; Li, W. C.; Spliethoff, B.; Schuth, F. Support effect in high activity gold catalysts for CO oxidation. *J. Am. Chem. Soc.* **2006**, *128,* 917–924.

[17] Iizuka, Y.; Tode, T.; Takao, T.; Yatsu, K.; Takeuchi, T.; Tsubota, S.; Haruta, M. A kinetic and adsorption study of CO oxidation over unsupported fine gold powder and over gold supported on titanium dioxide. *J. Catal.* **1999**, *187,* 50–58.

[18] Schwartz, V.; Mullins, D. R.; Yan, W. F.; Chen, B.; Dai, S.; Overbury, S. H. XAS study of Au supported on TiO_2: Influence of oxidation state and particle size on catalytic activity. *J. Phys. Chem. B* **2004**, *108,* 15782–15790.

[19] Beck, A.; Horvath, A.; Stefler, G.; Scurrell, M. S.; Guczi, L. Role of preparation techniques in the activity of Au/TiO_2 nanostructures stabilised on SiO_2: CO and preferential CO oxidation. *Top. Catal.* **2009**, *52,* 912–919.

[20] Soares, J. M. C.; Bowker, M. Low temperature CO oxidation on supported and unsupported gold compounds. *Appl. Catal. A-Gen.* **2005**, *291,* 136–144.

[21] Grunwaldt, J. D.; Kiener, C.; Wogerbauer, C.; Baiker, A. Preparation of supported gold catalysts for low-temperature CO oxidation via "size-controlled" gold colloids. *J. Catal.* **1999**, *181,* 223–232.

[22] Chou, J.; McFarland, E. W. Direct propylene epoxidation on chemically reduced Au nanoparticles supported on titania. *Chem. Commun.* **2004**, 1648–1649.

[23] Zheng, N.; Stucky, G. D. A general synthetic strategy for oxide-supported metal nanoparticle catalysts. *J. Am. Chem. Soc.* **2006**, *128,* 14278–14280.

[24] Yin, H. F.; Wang, C.; Zhu, H. G.; Overbury, S. H.; Sun, S. H.; Dai, S. Colloidal deposition synthesis of supported gold nanocatalysts based on Au–Fe_3O_4 dumbbell nanoparticles. *Chem. Commun.* **2008**, 4357–4359.

[25] Peng, S.; Lee, Y.; Wang, C.; Yin, H.; Dai, S.; Sun, S. A facile synthesis of monodisperse Au nanoparticles and their catalysis of CO oxidation. *Nano Res.* **2008**, *1,* 229–234.

[26] Zheng, N.; Fan, J.; Stucky, G. D. One-step one-phase synthesis of monodisperse noble-metallic nanoparticles and their colloidal crystals. *J. Am. Chem. Soc.* **2006**, *128,* 6550–6551.

[27] Shi, W.; Zeng, H.; Sahoo, Y.; Ohulchanskyy, T. Y.; Ding, Y.; Wang, Z. L.; Swihart, M.; Prasad, P. N. A general approach to binary and ternary hybrid nanocrystals. *Nano Lett.* **2006**, *6,* 875–881.

[28] Yu, H.; Chen, M.; Rice, P. M.; Wang, S. X.; White, R. L.; Sun, S. Dumbbell-like bifunctional Au–Fe_3O_4 nanoparticles. *Nano Lett.* **2005**, *5,* 379–382.

[29] Chen, M. S.; Goodman, D. W. Catalytically active gold: From nanoparticles to ultrathin films. *Acc. Chem. Res.* **2006**, *39,* 739–746.